The International Journal of Advanced Manufacturing Technology (2019) 100:3185–3195
https://doi.org/10.1007/s00170-018-2930-9

ORIGINAL ARTICLE

Analytical prediction of temperature in laser-assisted milling with laser preheating and machining effects

Yixuan Feng[1] · Tsung-Pin Hung[2] · Yu-Ting Lu[3] · Yu-Fu Lin[3] · Fu-Chuan Hsu[3] · Chiu-Feng Lin[3] · Ying-Cheng Lu[3] · Steven Y. Liang[1]

Received: 12 August 2018 / Accepted: 23 October 2018 / Published online: 29 October 2018

Abstract

An analytical predictive model for temperature in laser-assisted milling considering both laser preheating temperature and machining induced temperature rise is proposed. The preheating temperature at top surface is predicted first by considering the heat generation from laser and convection. The heat generation rate is described by Gaussian equation. Within the material, heat conduction is considered with isothermal boundary conditions at side and bottom surfaces. The machining temperature is considered by transferring the milling configuration to orthogonal cutting at each instance. The shearing heat source and secondary rubbing heat source are included for machining temperature prediction. The heat source is calculated from the cutting or plowing forces, and a mirror heat source method is applied to predict temperature rise through integration. The proposed model is validated through experimental measurements on silicon nitride ceramics and Ti-6Al-4V alloy. The proposed predictive model matches the experimental measurements with less than 7.1% difference at laser spot and 5.2% difference in front of the cutting zone with computation time less than 15 s. The model is valuable for providing a fast, credible, and physics-based method for the prediction of temperature in laser-assisted milling of various materials. The overall temperature distribution is accurately calculated by predicting laser preheating temperature and machining induced temperature rise.

Keywords Temperature · Modeling · Laser-assisted milling

Nomenclature

T_{laser}	Laser preheating temperature
ρ	Material density
c_p	Specific heat
h	Heat transfer coefficient
T_0	Environment temperature
q	Heat generation rate
Q	Total input power of laser
r	Radius of laser spot
α	Thermal diffusivity
V_f	Moving speed of laser spot/the feed speed
$\overline{t_c}$	Average depth of cut
RPM	Spindle speed
ϕ	Rotation angle
r_{corner}	Corner edge radius
Cs^*	Equivalent side cutting edge angle
F_c	Cutting force
F_t	Tangential force
d_a	Axial depth of milling
w^*	Equivalent orthogonal cutting width
t_c^*	Equivalent cutting depth
V_r	Cutting speed
R_t	Tool radius
P_{cut}	Plowing force in cutting direction
q_{shear}	Shearing heat source
φ	Shear angle
α^*	Equivalent rake angle
L_{AB}	Length of shear plane
k_{wk}	Thermal conductivity of workpiece
K_0	Neumann function
q_{rub}	Secondary rubbing heat source density
CA	Contact length
γ	Heat distribution coefficient

✉ Yixuan Feng
yfeng82@gatech.edu

[1] Woodruff School of Mechanical Engineering, Georgia Institute of Technology, Atlanta, GA 30332, USA

[2] Department of Mechanical Engineering, Cheng Shiu University, Kaohsiung, Taiwan

[3] Metal Industries Research and Development Centre (MIRDC), Kaohsiung, Taiwan

k_t, ρ_t, and C_t	Thermal conductivity, density, and specific heat of cutting tool
σ	Flow stress
σ_0	Yield stress
Q_{act}	Activation energy
R	Universal gas constant
T_m	Melting temperature

1 Introduction

Conventional milling on difficult-to-machine materials has become very challenging due to high tool wear and low material removal rate [1]. In order to improve the machinability of certain materials with high strength or hardness, people have been developing thermally enhanced machining methods for decades, among which laser-assisted machining is preferred because a highly concentrated heat source is able to control the preheating temperature field in an easier manner. Shi et al. [2] conducted numerical simulation on laser-assisted machining of Inconel 718, which indicated that the additional temperature increase in primary deformation zone due to laser effect would decrease the effective stress, and the reduced cutting force mainly resulted from the thermal softening effect on the flow stress. The cutting efficiency is therefore improved since the material removal rate could be increased while the cutting force and tool wear rate remain the same level. The high temperature could also benefit the surface quality. The edge chipping width decreases because of the dropped hardness as well as strength of workpiece material, and the machined surface is smoother with lower surface roughness [3]. On the other hand, the thermal loading in the cutting zone leads to tensile residual stresses. Therefore, the study of temperature in laser-assisted machining is critical for the guidance of process. The prediction of temperature is helpful finding the optimal combination of cutting parameters before the actual machining.

Milling process is more complex than most other machining processes in nature, and the temperature of laser-assisted milling process on various materials has been later investigated by different researchers. However, all these thermal analyses only consider the preheating temperature without actual material removal process. Wiedenmann and Zaeh [4] investigated temperature field in laser-assisted milling process. The assumption is made that the temperature distribution was independent from the milling operation. Therefore, the simulation only featured the interactions between laser and workpiece without material removal. Tian et al. [5] proposed thermal modeling of laser-assisted milling to predict temperature field by determining spatial distribution of the laser energy and heat transfer equations including conduction, convection, and radiation. Although good agreement was found, the validation heating tests were conducted without material removal. Therefore, only the laser preheating temperature was predicted without machining induced temperature rise. Bermingham et al. [6] measured temperature at laser focus and cutting tool in order to study the tool life and wear mechanisms in laser-assisted milling Ti-6Al-4V. Temperature signals were collected under different laser power and table speed, but only the laser traversed the surface of workpiece, and the temperature measured was preheating temperature instead of overall cutting temperature. Kim and Lee [7] did heat transfer analyses for laser-assisted milling of Inconel 718 and AISI 1045 steel using the finite element method. The static thermal analysis provided the effective depth of cut. Similarly, Woo and Lee [8] performed thermal analysis for the study of the machining characteristics of same materials in laser-assisted milling. The analysis addressed the conduction and heat generation rate due to laser, but the heat generated through machining was ignored, and only the preheating temperature was measured and studied. The negligence of machining effect is acceptable for some of these studies because the distance between laser beam and cutting edge is small. When the laser center is approximately at the tool tip and the laser power is high enough, the temperature rise due to machining is much smaller than laser preheating temperature and can be therefore ignored. However, this assumption is invalid under other conditions, and up to now, a comprehensive predictive model of temperature in laser-assisted milling process addressing both laser preheating temperature and machining induced temperature rise has not been proposed.

The temperature rise due to machining cannot be ignored in temperature prediction of laser-assisted milling process, especially when the laser-cutter allowance is large enough so that there is a significant drop of temperature from laser center to shear zone. According to the study of Navas et al. [9], the heat generated by plastic deformation in the primary shear zone would raise the local temperature of the material already preheated by the laser by another 100–150 °C for Inconel 718, where the laser preheating temperature measured at the point nearest to the cutting zone was around 500 °C. Therefore, the prediction of machining induced temperature rise needs to be considered since it could account for more than 30% of overall temperature. The study of predictive model of machining temperature in milling process can be tracked back to the year of 2000. Özel and Altan [10] predicted the temperatures in high-speed flat end milling using finite element analysis. The milling process was simplified to an orthogonal turning process assuming plane strain deformation. The trochoidal path traveled by the tip of cutting edge was assumed to be circular under small maximum undeformed chip thickness. Then, the flow stress was calculated by a constitutional model as a function of state variables. Abukhshim et al. [11] summarized the analytical models in temperature predictions of metal cutting in 2006. They concluded that purely analytical approaches were severely restrictive at that

time including the absence of heat source consideration and assumption of constant percentage of heat flow into chip and workpiece. Recently, Lu et al. [12] presented coupled thermal and mechanical analyses of micro-milling Inconel 718, where an iterative algorithm was proposed combining cutting force and temperature predictions. The cutting temperature significantly affects the shear stress which determines the cutting forces and plowing forces, while these forces are treated as two heat sources in temperature prediction. All these temperature prediction models due to machining have not been applied in laser-assisted milling and have not been combined with preheating temperature field.

It is concluded that the laser preheating temperature prediction has been established. However, the machining induced temperature rise is always ignored in laser-assisted milling. The machining temperature prediction models so far need to consider the milling configuration, the rubbing effect, the heat flow percentage into chip and workpiece, and coupled thermal and mechanical effects. The current study follows the same strategy of Özel and Altan [10] by transferring milling process to equivalent orthogonal cutting and applying state variables dependent flow stress predictive model [13]. Some issues raised by Abukhshim et al. [11] have also been addressed in current study by following the previous established machining temperature predictive model [14]. For example, the rubbing effect is considered as the secondary heat source, and the percentage of heat flow into chip and workpiece is determined by the thermal and mechanical properties of both tool and workpiece materials which are temperature dependent instead of a predefined constant. The current study follows Lu et al. [12] to include coupled thermal and mechanical effects while the laser preheating temperature is added. Overall, a comprehensive analytical model is proposed for temperature prediction in laser-assisted milling process. The laser preheating temperature is predicted through the previous established model [15] which firstly describes the heat source distribution through the laser total power input and then predicts the temperature rise considering conduction and convection. The laser preheating temperature is then embedded in machining temperature predictive model [14] considering the shearing and rubbing heat sources. The overall flowchart of the proposed model is presented in Fig. 1. For laser preheating temperature, plain strain condition is assumed, and heat transfer is only considered in cutting direction and depth direction. All the heat sources are assumed to be moving heat sources, and adiabatic uncut workpiece surface is assumed in machining temperature prediction. In Section 2, the prediction of laser preheating temperature field is presented. In Section 3, the prediction of machining induced temperature increase is presented. In Section 4, the model is validated through the comparison with results from experimental studies of laser-assisted milling of silicon nitride ceramics (Si_3N_4) [3, 16]

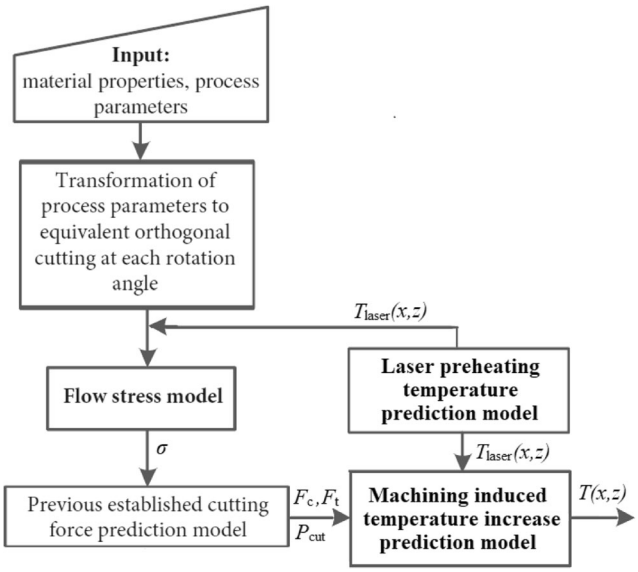

Fig. 1 Flowchart with input and output of the predictive model

and Ti-6Al-4V alloy [17], and the results of overall temperature predictions are discussed.

2 Temperature rise due to laser preheating

The laser-assisted milling is a complex machining process including the preheating of material ahead of tool tip by laser followed by the chip removal through the contact between tool tip and workpiece. Since the milling process is treated as equivalent orthogonal cutting process at each instance, plain strain condition is assumed, and heat transfer only occurs in cutting direction indicated by X and depth direction indicated by Z. The coordinate system is defined as in Fig. 2. The laser preheating temperature field is calculated considering heat generation by laser power at top surface of workpiece, convection between workpiece and environment at top surface, conduction within workpiece, and isothermal boundary

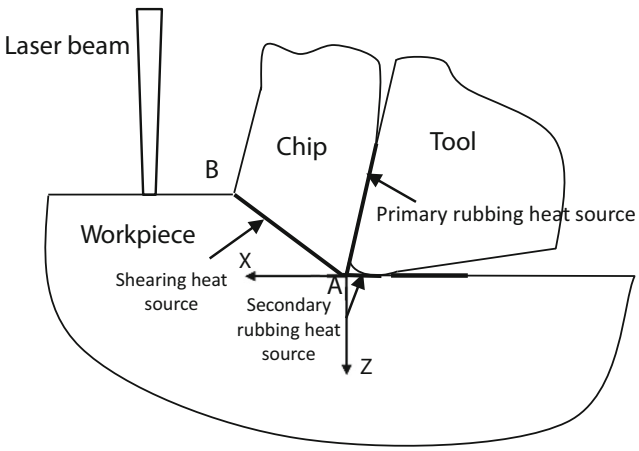

Fig. 2 Coordinate system and heat sources of the predictive model

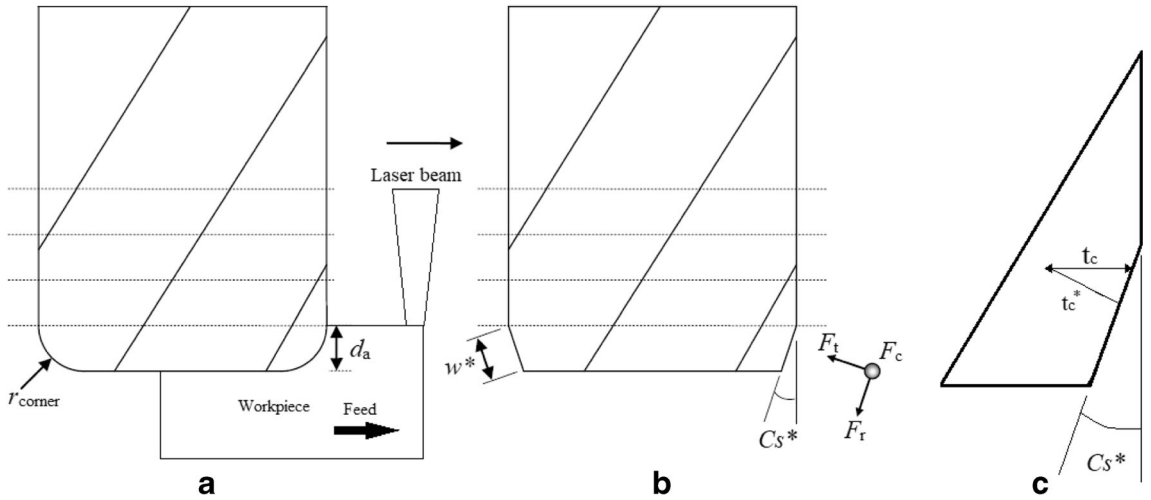

Fig. 3 Transformation from milling to equivalent orthogonal cutting. (a) Milling configuration with axial depth of milling d_a and tool edge radius r_{corner}. (b) Equivalent orthogonal cutting with equivalent side cutting edge angle Cs^* and equivalent cutting width w^*, the tangential cutting force is perpendicular to cutting edge instead of machined surface. (c) Transformation of cutting depth

conditions at both sides and bottom. The temperature increase rate at top surface is described by

$$\Delta T_{laser}(x,0) = \frac{q(x) - h(T_{laser}(x,0) - T_0)}{\rho c_p} \quad (1)$$

where T_{laser} is the laser preheating temperature, ρ is the material density, c_p is specific heat, h is the heat transfer coefficient, T_0 is the environment temperature, $q(x)$ is the heat generation rate due to laser power described by the Gaussian equation as

$$q(x) = \frac{2Q}{\pi r^2} \exp\left(-\frac{2x^2}{r^2}\right) \quad (2)$$

where Q is the total input power of laser, r is the radius of laser spot. Within the workpiece, heat conduction is the dominant effect with the governing equation of

$$\Delta T_{laser}(x,z) = \alpha \nabla^2 T_{laser}(x,z) - V_f \frac{\partial T_{laser}(x,z)}{\partial x} \quad (3)$$

where α is thermal diffusivity and V_f is the moving speed of laser spot or the feed speed. The first term on the right describes the two dimensional heat conduction, while the second term considers the effect of moving laser beam in cutting direction [15]. At side or bottom boundaries, isothermal condition is assumed in cutting direction. Therefore, heat conduction is only considered in Z direction as

$$\Delta T_{laser}(x,z) = \alpha \frac{\partial^2 T_{laser}(x,z)}{\partial z^2} \quad (4)$$

The workpiece is assumed to have same temperature as the environment as initial condition, which is 25 °C in the current study.

3 Machining induced temperature increase

After the preheating temperature being predicted, the cutting forces and plowing forces are calculated based on the flow stress model [18] dependent on state variables such as temperature, strain, and strain rate. The flow stress model is built

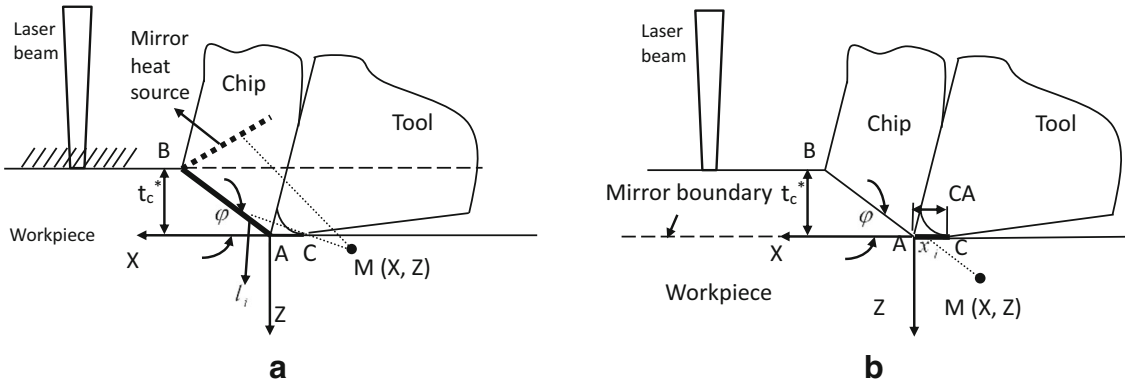

Fig. 4 Schematic of (a) shearing heat source and (b) rubbing heat source for machining temperature prediction [14]

Table 1 Constitutive model parameters for Si_3N_4 and Ti-6Al-4V

Si_3N_4	σ_0(MPa)	Q(KJ/mol)	R(J/mol·K)	ε_0	m	n	T(°C)	$\dot{\varepsilon}_0$ (s^{-1})
	25	800	8.31447	0.3	0.061	0.4	1400	1
Ti-6Al-4V	A(MPa)	B(MPa)	C	m	n	T_m(°C)	$\dot{\bar{\varepsilon}}_0$ (s^{-1})	
	997.9	653.1	0.0198	0.7	0.45	1668	1	

under the configuration of orthogonal cutting, which requires the transformation of milling process parameters including cutting depth, cutting width, side cutting edge angle, cutting speed, and so on. The modeling approach of milling in two dimensions is first proposed by Oxley [19]. This approach has been validated over time to be a practical methodology simplifying the milling configuration while still accurately describing the procedure. In milling process, the chips created during cutting do not remain the same thickness due to the geometry of milling tool. So for the equivalent orthogonal cutting model, the cutting depth will vary with rotation angle. The average depth of cut $\bar{t}_c$ is given as

$$\bar{t}_c = \frac{1}{2}\frac{V_f}{RPM} \tag{5}$$

where RPM is the spindle speed. Then the instantaneous equivalent cutting depth is,

$$t_c(\phi) = \sqrt{2} \times \bar{t}_c \times \sin(\phi) \tag{6}$$

where $\phi = 2\pi \times RPM \times t$ is the rotation angle at given time t.

As shown in Fig. 3(a), in milling process, a milling tool with corner edge radius of r_{corner} is simplified as an equivalent side cutting edge angle Cs^* indicated in Fig. 3(b). Therefore, for the equivalent orthogonal cutting, cutting force F_c and tangential force F_t are in the inclined cutting plane with Cs^* angle to horizontal plane. Therefore, for an axial depth of milling of d_a, the equivalent orthogonal cutting width w^* is calculated from the geometry shown in Fig. 3(c), as

$$w^* = \frac{d_a}{\cos(Cs^*)} \tag{7}$$

Moreover, the equivalent cutting depth t_c^* in orthogonal cutting also has an angle of Cs^* with t_c by

$$t_c^* = t_c(\phi) \times \cos Cs^* \tag{8}$$

The equivalent cutting speed is a function of rotation angle as,

$$V(\phi) = \sqrt{V_f{}^2 + V_r{}^2 + 2V_f V_r \cos\phi} \tag{9}$$

where $V_r = 2\pi R_t \times RPM$ is the cutting speed, R_t is the tool radius.

The rake angle and inclination angle of milling tool are transferred as well [13], and the preheating temperature is utilized to predict the flow stress that gives cutting force F_c,

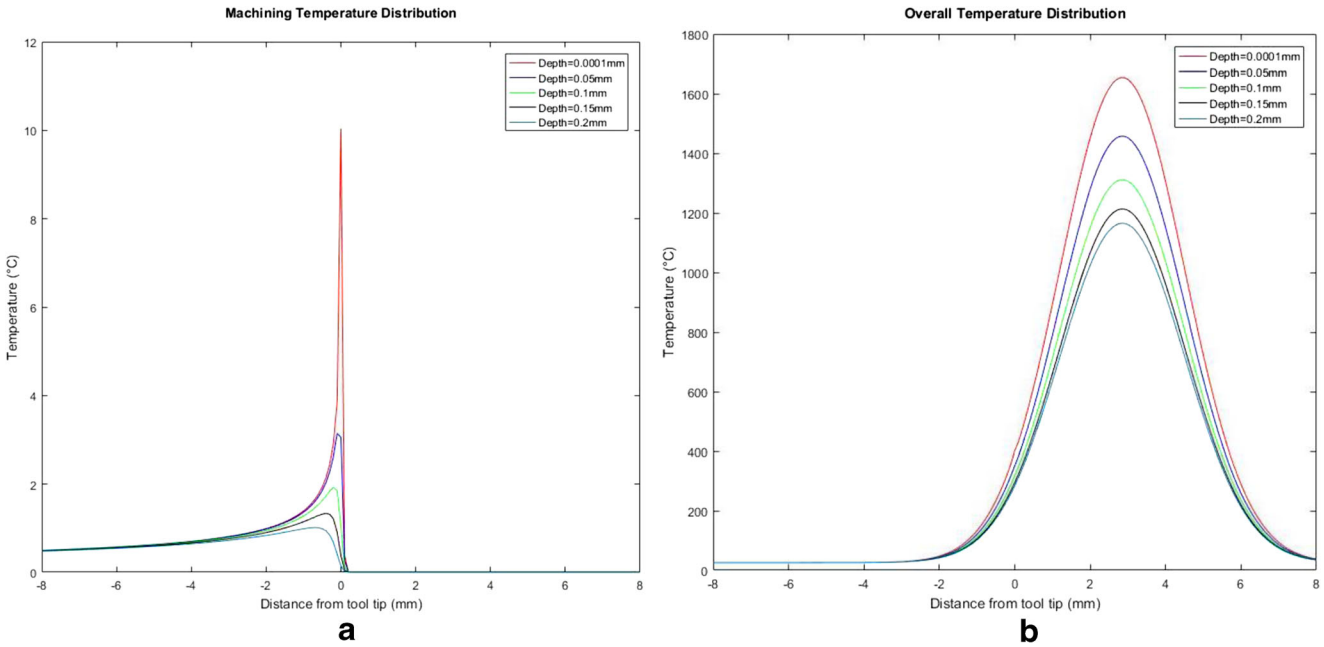

Fig. 5 Temperature field prediction of Si_3N_4 with laser power of 340 W and laser spot diameter 3.3 mm. (a) Machining induced temperature rise and (b) overall temperature distribution

Table 2 Temperature comparison for Si_3N_4 at 0.2 mm below machined surface under laser beam spot

Laser power (W)	Diameter of laser spot (mm)	Temperature measured from experiment (°C)	Temperature from the predictive model (°C)	Percentage difference (%)	Computation time (s)
300	3.3	About 1000	1031.00	3.10	3.09
340	3.3	About 1130	1165.13	3.11	2.94
410	3.3	About 1230	1246.37	1.33	2.91
340	1.8	About 1600	1713.27	7.08	2.92
340	2.6	About 1320	1341.21	1.61	2.91

tangential force F_t, and plowing force in cutting direction P_{cut} [18]. As shown in Fig. 2, three main heat sources contribute to the machining induced temperature rise. The plastic deformation in shear zone leads to the shearing heat source, while the friction on tool-chip interface and tool-workpiece interface induces two rubbing heat sources. The primary rubbing heat source is ignored because it mainly contributes to the temperature rise in chip instead of workpiece. Shearing heat source denoted by shear plane heat density q_{shear} is calculated from F_c and F_t by

$$q_{shear} = \frac{(F_c\cos\varphi - F_t\sin\varphi)(V(\phi)\cos\alpha^*/\cos(\varphi-\alpha^*))}{t_c^*\cdot w^*\cdot\csc\varphi} \quad (10)$$

where φ is the shear angle, α^* is the equivalent rake angle. A mirror heat source method is applied as shown in Fig. 4, when the moving heat sources and adiabatic uncut workpiece surface are assumed. In Fig. 4(a), a point on workpiece M(X, Z) is under a temperature rise from shearing heat source as well as its mirror heat source. The temperature rise at point M is calculated by

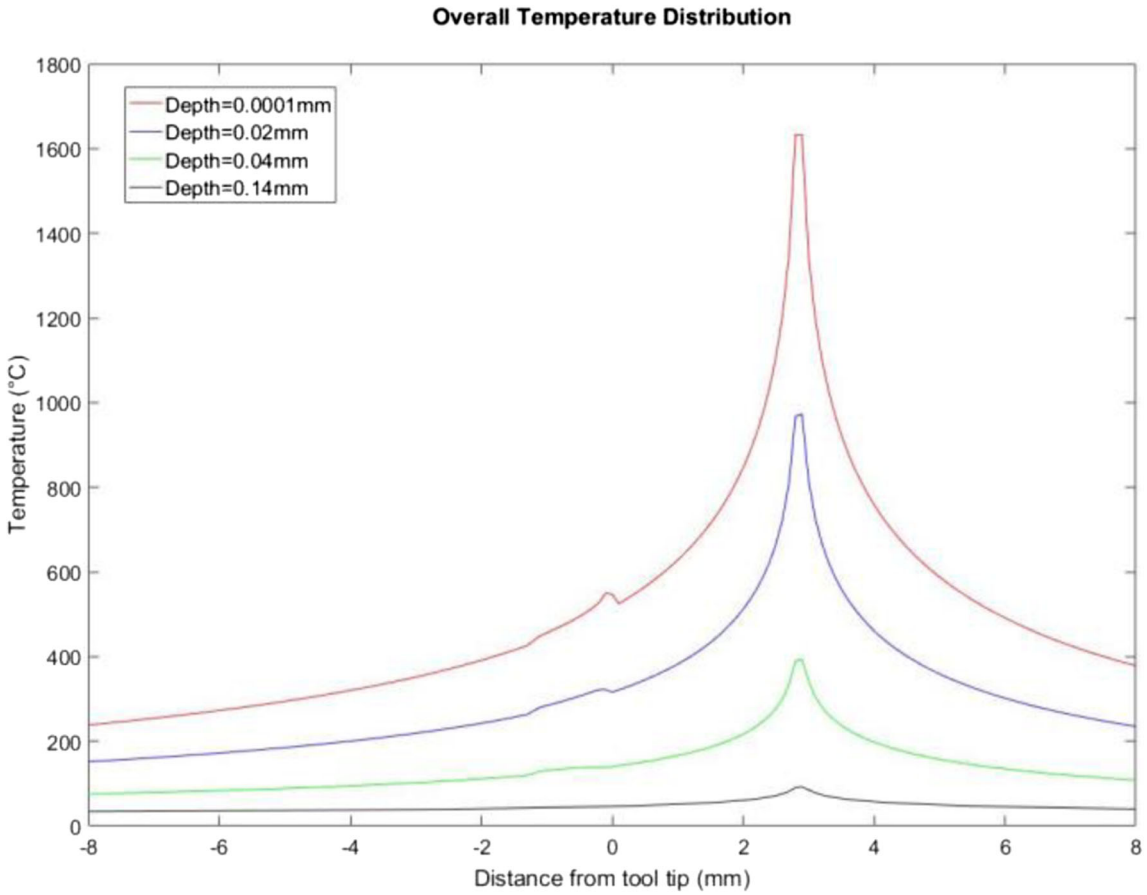

Fig. 6 Temperature field prediction of Ti-6Al-4V with laser power of 1250 W, cutting speed of 190 m/min, axial depth of cut of 1.5 mm, and laser-cutter allowance of 28.5 mm. The highest point in red curve corresponding to workpiece surface is compared with experimental measurement at the center of the laser spot at machined surface

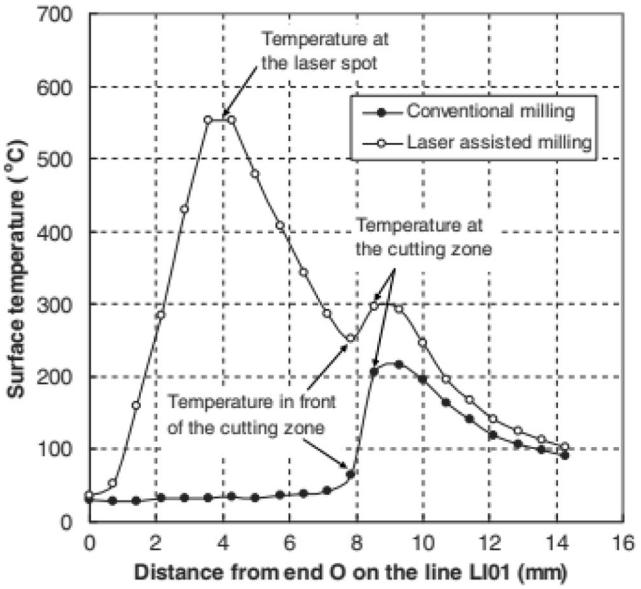

Fig. 7 Variation of surface temperature on the line L101 which goes through the laser spot and the cutting zone from experimental measurements [17]

$$\Delta T_{\mathrm{wk-shear}}(X,Z)=\frac{q_{\mathrm{shear}}}{2\pi k_{\mathrm{wk}}}\int_0^{L_{\mathrm{AB}}} e^{-\frac{(X-l_i\sin\varphi)V(\phi)}{2\alpha}}\left\{K_0\left[\frac{V(\phi)}{2\alpha}\sqrt{(X-l_i\cos\varphi)^2+(Z+l_i\sin\varphi)^2}\right]+K_0\left[\frac{V}{2\alpha}\sqrt{(X-l_i\cos\varphi)^2+(2t_c{}^*-l_i\sin\varphi+Z)^2}\right]\right\}dl_i \tag{11}$$

where $L_{\mathrm{AB}}=\frac{t_c{}^*}{\sin\varphi}$ is the length of shear plane, k_{wk} is the thermal conductivity of workpiece, and K_0 is the modified Bessel function of the second kind or Neumann function. The secondary rubbing heat source density q_{rub} comes from P_{cut} by

$$q_{\mathrm{rub}}=\frac{P_{\mathrm{cut}}V(\phi)}{w^*\cdot CA} \tag{12}$$

where CA is the contact length. As shown in Fig. 4(b), the secondary heat on tool-workpiece interface from rubbing is treated as a moving heat source along X direction. The temperature rise due to the rubbing is calculated as

$$\Delta T_{\mathrm{wk-rub}}(X,Z)=\frac{q_{\mathrm{rub}}}{\pi k_{\mathrm{wk}}}\int_0^{CA}\gamma e^{-\frac{(-X-x_i)V(\phi)}{2\alpha}}\left\{K_0\left(\frac{V(\phi)}{2\alpha}\sqrt{(X+x_i)^2+Z^2}\right)\right\}dx_i \tag{13}$$

where γ is a heat distribution coefficient defined as

$$\gamma=\frac{\sqrt{k_{\mathrm{wk}}\rho C_{\mathrm{p}}}}{\sqrt{k_{\mathrm{wk}}\rho C_{\mathrm{p}}}+\sqrt{k_{\mathrm{t}}\rho_{\mathrm{t}}C_{\mathrm{t}}}} \tag{14}$$

where k_{t}, ρ_{t}, and C_{t} are the thermal conductivity, density, and specific heat of cutting tool. Therefore, the temperature rise of any point on the workpiece M(X, Z) is calculated as the summation of two machining induced temperature rise sources in addition to laser preheating temperature rise,

$$\Delta T(X,Z)=\Delta T_{\mathrm{wk-shear}}(X,Z)+\Delta T_{\mathrm{wk-rub}}(X,Z)+\Delta T_{\mathrm{laser}}(X,Z) \tag{15}$$

4 Experimental validation and results

In order to validate the proposed predictive model, experimental measurements are collected during laser-assisted milling of Si_3N_4 [3] and Ti-6Al-4V [17].

4.1 Silicon nitride ceramics (Si_3N_4)

The laser-assisted milling is conducted on a CNC machine (Haas Automation Inc.). A diode laser (Visotek Inc., DFL500) in continuous-wave mode is used to generate a high-power laser beam. The surface temperature of the workpiece is measured through an infrared pyrometer (Williamson Inc., Model 91-20-C-23D) with a range from 475 to 1750 °C. The dimensions of Si_3N_4 specimens are 4.3 × 5.3 × 48 mm. The axial depth of cut is 1 mm, the feed speed is 6 mm/min, and the laser-cutter allowance or the distance between laser beam spot and tool tip is about 3 mm. The pyrometer measures the temperature at about 0.2 mm below the machined surface corresponding to the laser beam spot. Measurements from five experiments are compared with two variables including diameter of laser spot and laser power. For the first three experiments, the diameter of laser spot is a constant of 3.3 mm with three levels of laser power 300, 340, and 410 W. The other two experiments have a constant laser power of 340 W with different diameters of laser spots of 1.8 and 2.6 mm. The predictive model introduces a constitutive model for flow stress [16] following the form of

$$\sigma=\sigma_0\left\{1+\left(\frac{\varepsilon}{\varepsilon_0}\right)^n\right\}\left\{\frac{\dot{\varepsilon}}{\dot{\varepsilon}_0}\cdot exp\left(\frac{Q_{\mathrm{act}}}{RT}\right)\right\}^m \tag{16}$$

where σ_0 is the yield stress measured at $\dot{\varepsilon}=1\times10^{-8}s^{-1}$, Q_{act} is the activation energy, and R is the universal gas constant. All the material constants are listed in Table 1.

As shown in Fig. 5, the temperature distribution from the predictive model is able to show both the machining induced temperature rise and overall temperature including laser effect, when the laser power is 340 W and laser spot dimeter is 3.3 mm. The machining induced temperature rise is negligible for Si_3N_4, because the maximum temperature rise at tool tip is only 10.04 °C at machined surface as shown in Fig. 5(a). The overall maximum temperature occurs at 3 mm ahead of tool tip due to laser-cutter allowance as shown in Fig. 5(b). The temperature distribution at depth of 0.2 mm below machined surface is compared with experimental measurements as listed in Table 2. The

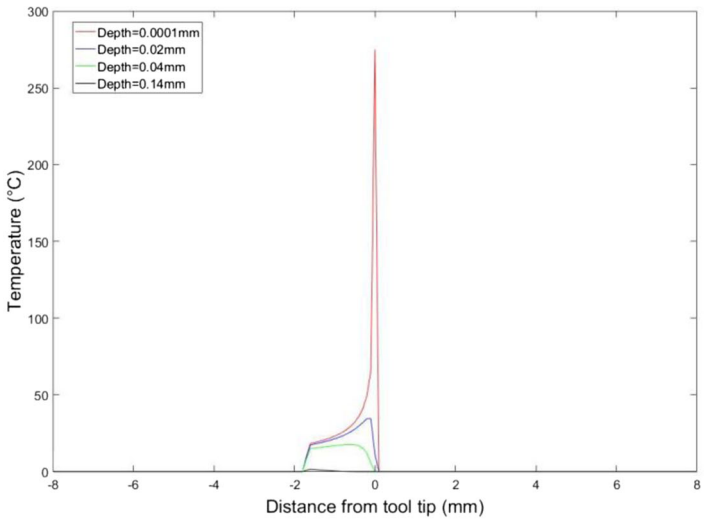

(a)

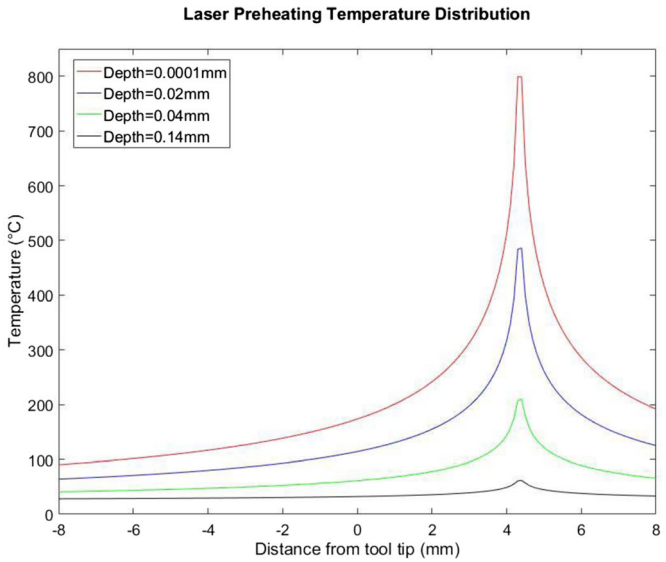

(b)

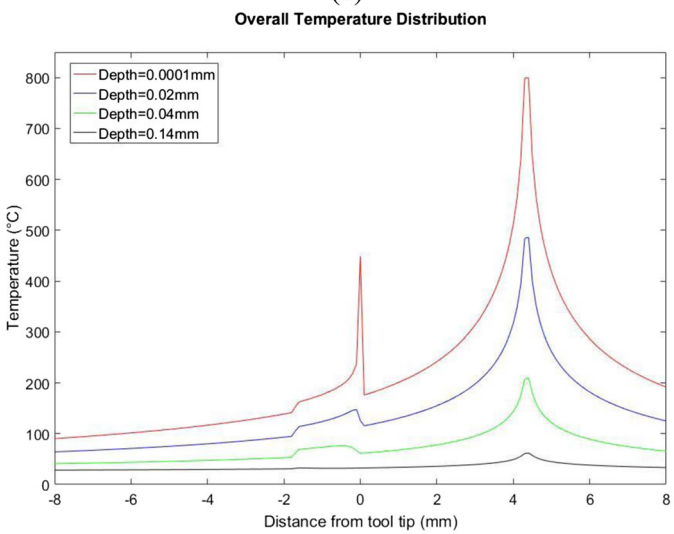

(c)

Fig. 8 Temperature field prediction of Ti-6Al-4V with laser power of 510 W, cutting speed of 130 m/min, axial depth of cut of 1 mm, and laser-cutter allowance of 43.5 mm. (a) Machining induced temperature rise, (b) laser preheating temperature field, and (c) overall temperature distribution

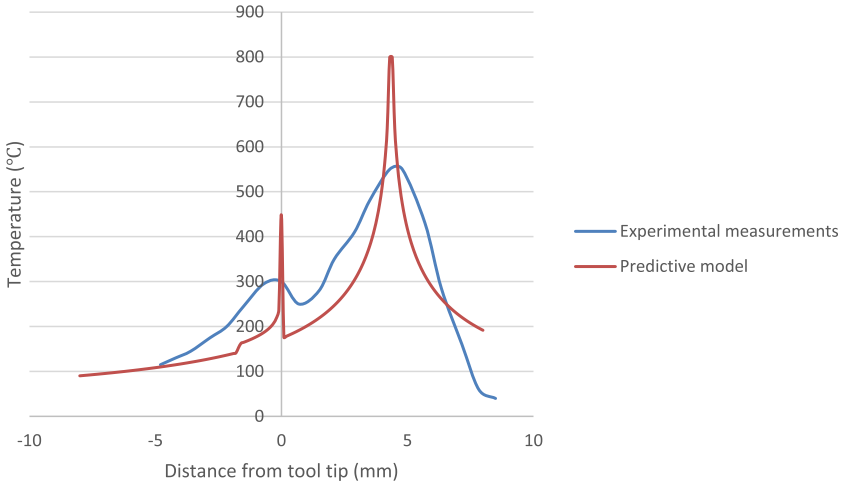

Fig. 9 Comparison between experimental measurements and predictive model. The predicted temperature profile is from the red curve in Fig. 8(c), while experimental measurements are from the line L101 shown in Fig. 7

temperature below laser spot increases with a larger laser power or a smaller laser spot diameter, which matches the prediction of the proposed model. Good agreements are found for the maximum temperature prediction between experimental measurements and the predictive model with average difference of 3.25% and maximum difference of 7.08%. The prediction process is done within 3.1 s for all cases.

4.2 Ti-6Al-4V

The experiments are conducted on a 5-hp Hafco Metal Master mill with model BM-62VE under dry conditions. The cutter is a 490-040C40-0M type with a diameter of 40 mm and four carbide inserts. The tool has a primary rake angle of 30° and clearance angle of 6°. A continuous-wave Nd:YAG laser with wavelength 1.064 μm and maximum power 2.5 kW is used. The diameter of laser spot is 5 mm, and the feed rate is 0.1 mm/tooth. A Maurer model QKTR 1075 two-color optical pyrometer and an infrared thermal camera of ThermoVision® model A40 are applied to measure the surface temperature at the laser spot. The measurement range for the pyrometer is between 800 and 2500 °C and for the infrared thermal camera is up to 2000 °C. The flow stress constitutive model for Ti-6Al-4V applied in the predictive model follows the equation of

$$\sigma = \left(A + B\bar{\varepsilon}^{n}\right)\left(1 + C\ln\frac{\dot{\bar{\varepsilon}}}{\dot{\bar{\varepsilon}}_0}\right)\left\{1-\left(\frac{T-T_0}{T_m-T_0}\right)^{m}\right\} \quad (17)$$

where T_m is the melting temperature and T_0 is the environment temperature. All the material constants are listed in Table 1.

The first measurement is collected at laser spot at cutting speed of 190 m/min, axial depth of cut of 1.5 mm, feed speed of 600 mm/min, laser-cutter allowance of 28.5 mm, and laser power of 1250 W. The temperature distribution from the predictive model is shown in Fig. 6. At the center of the laser spot at machined surface, a constant value of 1550 °C is recorded after the laser beam fully interacting with the workpiece. The maximum temperature at surface from the predictive model is 1633.39 °C. The difference is 5.38% and the computation time is 6.73 s.

In order to check the variation of surface temperature near the cutting zone, an infrared thermal camera with different set up range from 0 to about 500 °C is applied to record the temperature in the middle of the radial depth of cut going through both the laser spot and the cutting zone. The cutting speed is 130 m/min, axial depth of cut is 1 mm, feed speed is 400 mm/min, laser-cutter allowance is 43.5 mm, and laser power is 510 W. The profile of temperature distribution by connecting measured points from experiments is shown in Fig. 7. The temperature at the laser spot is cut off because the upper limit of measurement range is reached. Since the laser-cutter allowance is larger and the laser power is lower, the machining induced temperature rise cannot be ignored at the cutting zone. The temperature in front of the cutting zone is 250 °C, while the temperature at the cutting zone is about 300 °C, which indicates that the contribution of the machining process to the temperature increase at the cutting zone is about 50 °C. Under same conditions, the predicted temperature profiles from proposed analytical model at different depths are shown in Fig. 8. From Fig. 8(a), the maximum temperature rise at surface is 274.89 °C, while the corresponding laser preheating temperature is 173.65 °C from Fig. 8(b). Therefore, the machining induced temperature rise has a more significant effect at the cutting zone than laser. By comparing overall temperature distribution from Fig. 8(c) to Fig. 7, as shown in Fig. 9, the temperature in front of the cutting zone from the predictive model is 237.18 °C with a 5.13% difference from experiments. The predicted temperature at the cutting zone is 448.54 °C, which is much higher than the experimental measurement. The main reason is the lack of measurement points at the cutting zone. As seen in Fig. 7, there are only two data points connected by a smooth curve. However,

in the profile from the predictive model, there is a rapid rise of temperature over 200 °C followed by a sudden drop within 0.2 mm at the cutting zone. The density of measurement points at the cutting zone is unable to capture this trend. Overall, the predictive model catches the temperature distribution measured by experiments except for extreme points at the laser spot and the cutting zone due to the lack of measurements. The computation time is 14.67 s.

5 Conclusions

An analytical predictive model for temperature in laser-assisted milling considering both laser preheating temperature and machining induced temperature rise is proposed. The laser preheating temperature field is predicted in cutting and depth directions. The top surface is predicted first by considering the heat generation from laser and convection. The heat generation rate is described by Gaussian equation. Within the material, heat conduction is considered with isothermal boundary conditions at side and bottom surfaces. The machining temperature is considered by transferring the milling configuration to orthogonal cutting at each instance. All process parameters including cutting depth, cutting speed, and tool geometry are recalculated. The shearing heat source and secondary rubbing heat source are included for machining temperature prediction. The heat source is calculated from the cutting or plowing forces, and a mirror heat source method is applied to predict temperature rise through integration. The proposed model is validated through experimental measurements on Si_3N_4 and Ti-6Al-4V. The following conclusions are summarized:

- The machining induced temperature rise is negligible comparing to laser preheating temperature under certain combination of material and process parameters. The temperature will then only depend on laser configuration which increases with a larger laser power or a smaller laser spot diameter.
- The machining induced temperature rise cannot be ignored under certain cases especially at the cutting zone, when the laser power is low or the laser-cutter allowance is large.
- The proposed predictive model matches the experimental measurements with less than 7.1% difference at the laser spot and 5.2% difference in front of the cutting zone. A good agreement is also found between the profiles of temperature distribution from experiments and the predictive model.

The proposed analytical model is valuable for providing a fast, credible, and physics-based method for the prediction of temperature in laser-assisted milling of various materials. The overall temperature distribution is accurately calculated by predicting laser preheating temperature and machining induced temperature rise.

References

1. Doukas C, Stavropoulos P, Papacharalampopoulos A, Foteinopoulos P, Vasiliadis E, Chryssolouris G (2013) On the estimation of tool-wear for milling operations based on multi-sensorial data. Procedia CIRP 8:415–420
2. Shi B, Attia H, Vargas R, Tavakoli S (2008) Numerical and experimental investigation of laser-assisted machining of Inconel 718. Mach Sci Technol 12(4):498–513
3. Shen X, Lei S (2010) Experimental study on operating temperature in laser-assisted milling of silicon nitride ceramics. Int J Adv Manuf Technol 52(1–4):143–154
4. Wiedenmann R, Zaeh MF (2015) Laser-assisted milling—process modeling and experimental validation. CIRP J Manuf Sci Technol 8:70–77
5. Tian Y, Wu B, Anderson M, Shin YC (2008) Laser-assisted milling of silicon nitride ceramics and Inconel 718. J Manuf Sci Eng 130(3):031013
6. Bermingham MJ, Sim WM, Kent D, Gardiner S, Dargusch MS (2015) Tool life and wear mechanisms in laser assisted milling Ti–6Al–4V. Wear 322-323:151–163
7. Kim D-H, Lee C-M (2014) A study of cutting force and preheating-temperature prediction for laser-assisted milling of Inconel 718 and AISI 1045 steel. Int J Heat Mass Transf 71:264–274
8. Woo W-S, Lee C-M (2015) A study of the machining characteristics of AISI 1045 steel and Inconel 718 with a cylindrical shape in laser-assisted milling. Appl Therm Eng 91:33–42
9. Garcí et al (2013) Mechanisms involved in the improvement of Inconel 718 machinability by laser assisted machining (LAM). Int J Mach Tools Manuf 74:19–28
10. Özel T, Altan T (2000) Process simulation using finite element method — prediction of cutting forces, tool stresses and temperatures in high-speed flat end milling. Int J Mach Tool Manu 40:713–738
11. Abukhshim NA, Mativenga PT, Sheikh MA (2006) Heat generation and temperature prediction in metal cutting: a review and implications for high speed machining. Int J Mach Tools Manuf 46(7–8): 782–800
12. Lu X, Wang H, Jia Z, Feng Y, Liang SY (2018) Coupled thermal and mechanical analyses of micro-milling Inconel 718. Proc Inst Mech Eng B J Eng Manuf:095440541877458
13. Pan Z, Feng Y, Lu YT, Lin YF, Hung TP, Hsu FC, Liang SY (2017) Force modeling of Inconel 718 laser-assisted end milling under recrystallization effects. Int J Adv Manuf Technol 92:2965–2974
14. Feng Y, Pan Z, Liang SY (2018) Temperature prediction in Inconel 718 milling with microstructure evolution. Int J Adv Manuf Technol 95(9–12):4607–4621
15. Pan Z, Feng Y, Hung TP, Jiang YC, Hsu FC, Wu LT, Lin CF, Lu YC, Liang SY (2017) Heat affected zone in the laser-assisted milling of Inconel 718. J Manuf Process 30:141–147
16. Tian Y, Shin YC (2007) Multiscale finite element modeling of silicon nitride ceramics undergoing laser-assisted machining. J Manuf Sci Eng 129(2):287

17. Sun S, Brandt M, Barnes JE, Dargusch MS (2011) Experimental investigation of cutting forces and tool wear during laser-assisted milling of Ti-6Al-4V alloy. Proc Inst Mech Eng B J Eng Manuf 225(9):1512–1527
18. Pan Z, et al. (2017) Turning force prediction of AISI 4130 considering dynamic recrystallization. (50725): p. V001T02A040
19. Oxley PLB (1989) Mechanics of machining, an analytical approach to assessing machinability: ELLIS HORWOOD LIMITED. 242